



The activity of ALD-prepared PtCo catalysts for ethanol oxidation in alkaline media



A. Santasalo-Aarnio^{a,*}, E. Sairanen^b, R.M. Arán-Ais^c, M.C. Figueiredo^a, J. Hua^d, J.M. Feliu^c, J. Lehtonen^b, R. Karinen^b, T. Kallio^a

^a Research Group of Fuel Cells, Aalto University, P.O. Box 16100, 00076 Aalto, Finland

^b Industrial Chemistry Research Group, School of Chemical Technology, Aalto University, P.O. Box 16100, 00076 Aalto, Finland

^c Instituto de Electroquímica, Universidad de Alicante, Apartado 99, 03080 Alicante, Spain

^d NanoMaterials Group, Department of Applied Physics, Aalto University, Espoo, Finland

ARTICLE INFO

Article history:

Received 14 June 2013

Revised 20 August 2013

Accepted 20 August 2013

Keywords:

Ethanol oxidation

ALD

PtCo catalyst

Temperature dependency

DEFC

Alkaline media

FTIR

Arrhenius plot

ABSTRACT

Controlled bimetallic catalyst materials can be obtained using atomic layer deposition (ALD) method. In this paper, this method was applied to prepare Pt, PtCo, and PtCoPt nanoparticle catalysts on carbon support. Their activity for ethanol oxidation was studied by various electrochemical methods and the dependency of the reaction on temperature and mass transfer was evaluated. In addition, FTIR analysis was performed to confirm the reaction products. The results showed that bimetallic PtCo enhances ethanol oxidation by increasing the amount of CO₂ produced; however, at elevated temperatures, the bimetallic PtCo catalyst lacked stability. Nevertheless, the ALD-prepared PtCoPt catalyst showed similar reaction mechanism as PtCo catalyst, but possess increased stability and superior performance for ethanol oxidation at elevated temperatures.

© 2013 Elsevier Inc. All rights reserved.

1. Introduction

Polymer electrolyte fuel cells (PEFC) have been studied intensively for decades. However, real commercial breakthrough has not been attained due to the expensive cell components including the catalyst materials and the membrane used as an electrolyte. For low power demand applications such as laptops, alcohols are interesting fuels due to their high energy density and easy storage compared to the gaseous hydrogen. From organic alcohols, mostly methanol is currently used in fuel cell applications. However, it is toxic, easily flammable and as a small molecule has a tendency to permeate the electrolyte membrane reducing the overall efficiency. Conversely, ethanol is non-toxic, can be produced from biomass, and has both higher boiling point and theoretical energy density [1] compared to methanol. In addition, as larger molecule ethanol has reduced crossover rate through both proton and anion exchange membranes [2,3] making it an attractive fuel for direct ethanol fuel cells (DEFC).

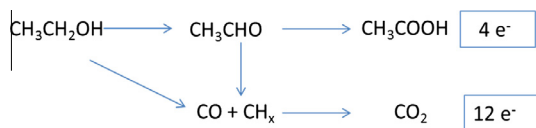
Nevertheless, with all organic fuels, some challenges are faced: Firstly, reaction kinetics of alcohol oxidation is sluggish and

therefore the power density obtained from the cell is moderate. Secondly, only diluted alcohol solutions can be used due to the severe crossover of the fuel to the cathode leading mixed potentials lowering the total performance. It has been known for decades that alcohol oxidation kinetics is enhanced in alkaline media compared to acidic [4–7], and therefore, lower amount of expensive noble metal catalyst is needed reducing the cost of the total system remarkably. The lack of anion exchange membrane materials has limited the research in alkaline media; however, in recent years, these membranes have been developed and demonstrated successfully in fuel cells [8–13].

The oxidation of ethanol can occur *via* a dual path mechanism involving production of 4 or 12 electrons [5,14–16] that is illustrated in Scheme 1. According to the 4 e⁻ path, adsorbed ethanol molecule is oxidized to acetaldehyde producing two protons and electrons and can be further oxidized to acetic acid producing two more protons and electrons. With this, 4 e⁻ path ethanol molecule is only partly oxidized and the final product is an organic acid that is a problematic in fuel cell conditions because it effects the local pH in the electrode layer. As can be seen in Scheme 1, the other path includes the cleavage of C–C bond from either adsorbed ethanol or acetaldehyde forming CO and CH_x fragments which can both further be oxidized to CO₂. This path produces 12 protons and

* Corresponding author.

E-mail address: annukka.aarnio@iki.fi (A. Santasalo-Aarnio).



Scheme 1. The oxidation paths of ethanol.

electrons implying that from the same molecule, two to three times higher current can be generated increasing significantly the total efficiency of the system.

Platinum is generally considered as the best monometallic catalyst for the oxidation of small organic molecules due to its capability to catalyze C–H bond rupture at comparatively low overpotential. Nevertheless, ethanol oxidation involves other reaction steps such as C–C bond cleavage and CO or acetaldehyde oxidation, and therefore, for total oxidation, high overpotentials are required. On pure Pt catalyst, the ethanol oxidation follows mostly the $4 e^-$ path [17] and therefore the demand for bimetallic catalyst is evident. For instance, PtRu has been found to be an excellent catalyst for methanol oxidation [18], because Ru allows water molecules to break forming OH groups on its surface at low overpotentials that is needed for the total oxidation of methanol [19]. Unfortunately, this catalyst has not shown ability to break the C–C bond and is, therefore, considered to be a good catalyst only for molecules with single carbon. Despite the vast effort, a catalyst material that could oxidize ethanol efficiently to CO_2 in acidic media has not been discovered. However, in alkaline media, the reaction mechanisms are different, and in addition, many oxides and alloys are stable at wider potential range. PtCo catalyst has traditionally been studied for oxygen reduction reaction both in acidic and alkaline media [20–22]. Recently, few studies with this catalyst have been performed for alcohol oxidation [23–28] and this bimetallic catalyst has shown decrease in onset potential and increase in oxidation currents of alcohols especially at low potentials. Nevertheless, most of these studies are made in acidic media where the dissolution of Co is likely at 0.4–0.8 V [27] which are relevant potentials for DEFC anode operation.

Unfortunately, the preparation of bimetallic catalyst is challenging: to ensure high catalytic activity, the metal particles should be in near vicinity of each other and not as separate islands. With traditional impregnation method, most commonly involving metal salt reduction on carbon powder in a solvent, the metal distribution control is poor resulting in increased noble metal catalyst loading that prevents the commercialization of the DEFC technology. Conversely, with atomic layer deposition (ALD), the metal precursors are vaporized to gas phase and flowed through the porous carbon support. This support is hydrophobic and therefore most of the atoms rather attach to hydrophilic defects on the support. When preparing bimetallic catalysts by the ALD method, a single metal precursor forms metallic nanoparticles on support with the first ALD cycles. After these cycles, the second metal is introduced attaching to the first metal or to the carbon support. The nanoparticle size and loading can be controlled by varying the ALD cycle variables [29]. Overall, with the ALD method, very uniformly distributed monometallic [30–33] and bimetallic [34–36] catalyst has been reported possessing high catalytic activity in comparison with catalysts produced with traditional methods. However, no ALD-prepared bimetallic catalyst for ethanol oxidation has been previously reported.

In this study, ALD-prepared Pt and PtCo catalytic materials are introduced and their activity toward ethanol oxidation in alkaline media is studied with electrochemical methods including cyclic voltammetry as well as long- and short potential step experiments. To understand the reaction mechanism occurring on the catalyst

surfaces, a FTIR analysis of the reaction intermediates and products was performed further facilitating the analysis of the electrochemical data. In addition, the activity for ethanol oxidation was evaluated as a function of operation temperature providing important knowledge for the catalyst activity in real fuel cell systems.

2. Experimental

2.1. Catalyst preparation

ALD catalysts were prepared in a commercial flow-type ALD reactor (F-120, ASM Microchemistry) applying pressure of 0.5–1 kPa. Carbon black was used as catalyst support (Vulcan XC72R, Cabot GR-3875) and platinum acetylacetonate, $\text{Pt}(\text{acac})_2$ (Volatec Oy) as well as cobalt acetylacetonate, $\text{Co}(\text{acac})_3$ (Merck, 98%) were applied as metal precursors. The catalyst preparation cycle consisted of three steps: first, the catalyst support was dried in N_2 flow (AGA, 99.999%) at 180 °C for 5 h. Second, the metal precursor was evaporated and fed on the support using N_2 carrier gas at 180 °C for 6 h in reduced pressure. Third, the unreacted precursor was flushed from the support with N_2 and reactor was cooled down to room temperature under N_2 flow. Reaction cycles were repeated to prepare bimetallic catalysts with additional Co or Pt cycles. A commercial 20 wt% Pt on a carbon support (Alfa Aesar) was used as a reference material.

The prepared catalyst was characterized by atomic emission spectroscopy (AES) (ICP-AES Varian Liberty series II) to determine the total metal loadings. A double-aberration corrected JEOL 2200FS (JEOL, Japan) high-resolution transmission electron microscope (HRTEM) was used to characterize the particle size distribution. The microscope is equipped with a field emission gun (FEG) operated at 200 kV and an energy dispersive X-ray (EDX) spectrometer for elemental analysis. A Gatan 4kx4k UltraScan 4000 CCD camera was employed for digital recording of HRTEM images. Gatan Digitalmicrograph software was used for camera control and image processing. The mean particle size was evaluated by analyzing 150–250 particles.

2.2. Electrochemical measurements

The catalyst inks were prepared with 5 mg of the catalyst powder that was dissolved in 200 μl *n*-methyl-2-pyrrolidone (Merck) following by the addition of 6 μl of fumion® FAA-3 ionomer dispersion (FumaTech). The ink was left under mixing with a magnetic stirrer for 2 h and sonicated with an ultrasonic bath for 40 min. The surface of glassy carbon electrode was cleaned mechanically by alumina slurry and ultrasonic bath. 3 μl droplet of the catalyst ink was spread on the electrode and was dried for 1 h at 60 °C in a vacuum oven. The electrochemical activity of the catalysts was studied in a three electrode electrochemical cell presented in Fig. 1. The previously mentioned glassy carbon electrode was used as a working electrode (WE) attached with a rotating device (Pine instruments), a large platinum wire was used as the counter electrode (CE), and a reversible hydrogen electrode (RHE) was used as a reference electrode (RE). Freshly prepared 0.1 M NaOH solution (Merck) was used as electrolyte, and all the solutions were made using MQ water (Millipore, 0.04 $\mu\text{S cm}^{-1}$).

The surface potential of the working electrode was controlled during the experiments to avoid unwanted anion adsorption, and the temperature of the electrochemical cell was adjusted with a water jacket controlled by CH cryostat/thermostat (Haake). Prior to the experiments, the electrolyte was deaerated by purging with N_2 and the temperature was stabilized to 20 °C. During the measurements, the gas stream was directed above the solution surface. The experiments were performed by a potentiostat/galvanostat

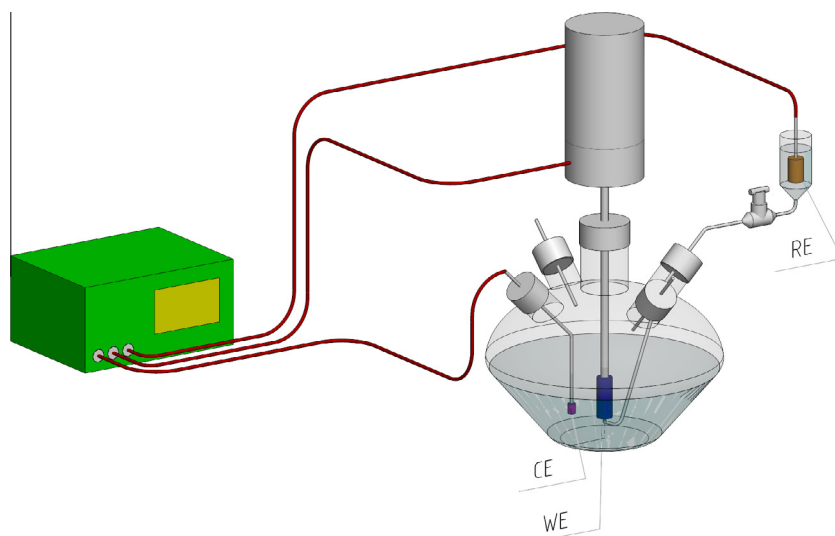


Fig. 1. The electrochemical cell with three electrodes: working electrode (WE), counter electrode, (CE) and reference electrode (RE).

PGSTAT100 Autolab system. Firstly, a cyclic voltammogram (50 mV s^{-1}) was obtained to ensure that the electrode preparation has succeeded. The catalyst surface cleaning was done with CO adsorption/oxidation method to avoid cycling to high potentials that could cause Co dissolution and Pt particle agglomeration. The electrolyte was purged with CO gas (Aga, 3.7), while the potential of the working electrode was cycled between 0.1 and 0.35 V to observe the blocking of the Pt site. When no further decrease in current was observed, the potential was fixed to 0.1 V and the gas was changed to N_2 and purged for 20 min to remove CO from the electrolyte. Subsequently, a cyclic voltammogram with CO oxidation was obtained with 10 mV s^{-1} . After these cyclic voltammograms of the clean catalyst surface were obtained at 20 mV s^{-1} . All potentials were scaled to reversible hydrogen electrode (RHE) scale, and all currents were normalized by the electrochemical active surface area obtained from surface area integrated from the first and last scans during the CO adsorption in the potential range from 0.1 to 0.35 V.

After the measurements in the pure electrolyte, ethanol (Altia, p.a.) was added to the cell to obtain 1 mol dm^{-3} ethanol solution. To prevent the changes in the concentration, the gas inlet was first directed into a bubbler bottle containing the same solution as the cell and alcohol-saturated gas was directed to the experimental cell. Cyclic voltammograms were recorded at 10 mV s^{-1} rate with 0 and 1800 rpm rotation at various temperatures (0, 20, 40, and 60°C). To further study the catalyst poisoning, chronoamperometric measurements were performed. These phenomena were studied with long (30 min) constant potential experiments at 0.5 V potential that still is relevant for DEFC anodes [37] and with short experiments of 5 min at various potentials.

2.3. Reaction product analysis by FTIR

As reported elsewhere [38,39], spectroelectrochemical experiments were performed with a Nicolet Magna 850 spectrometer equipped with a MCT detector. The spectroelectrochemical cell was provided with a prismatic CaF_2 window beveled at 60° . Spectra shown are composed of 100 interferograms collected with a resolution of 8 cm^{-1} and p-polarized light. They are presented as absorbance, according to

$$A = -\log \frac{R}{R_0} \quad (1)$$

where R and R_0 are the reflectance corresponding to the single beam spectra obtained at the sample and reference potentials, respectively. All the spectroelectrochemical experiments were performed at room temperature, with a RHE and a platinum wire used as reference and counter electrodes, respectively. The attenuated total reflection (ATR) spectra were collected using a SeZn hemicylindrical window with an incident angle of 60° . One hundred scans were collected with a resolution of 8 cm^{-1} . The reference spectra were acquired with a 0.1 M NaOH solution.

3. Results and discussion

3.1. Physical characterization

ALD method was used to prepare a set of mono- and bimetallic nanoparticle catalysts on a carbon support by varying the order of metal depositions to obtain Pt, PtCo, and PtCoPt catalyst where the catalyst name indicates the deposition order of the elements. The metal contents of all the ALD-prepared catalyst were determined with AES, and these values are presented in Table 1 together with the mean particle size obtained from HRTEM images (Fig. 2). The obtained noble metal loadings are low 5–15 wt% as desired for DEFC applications. The Pt (ALD) and PtCo (ALD) catalysts originate from the same catalyst batch, and they were prepared so that after the ALD cycles of Pt, part of the catalyst material was removed from the reactor. Subsequently, half of the Pt (ALD) material was replaced to the reactor and Co cycles were performed. For this reason, Pt (ALD) and PtCo (ALD) catalysts have the same Pt/C ratio. It has been previously shown that a noble metal layer on top of a less noble metal decreases dissolution of the latter [27], and therefore, three ALD depositions cycles in the order of Pt, Co, and Pt were applied for one catalyst sample. Due to the sample amount requirements, PtCoPt (ALD) catalyst was prepared from a different batch

Table 1
The catalysts metal loadings and the mean particle sizes analyzed by AES and TEM, respectively.

	Pt (wt%)	Co (wt%)	Co/Pt ratio	Particle size (nm)
Pt (Com)	20.00	–	–	2.30
Pt (ALD)	13.97	–	–	2.00
PtCo (ALD)	13.78	1.38	0.10	2.64
PtCoPt (ALD)	8.06	0.79	0.10	1.68

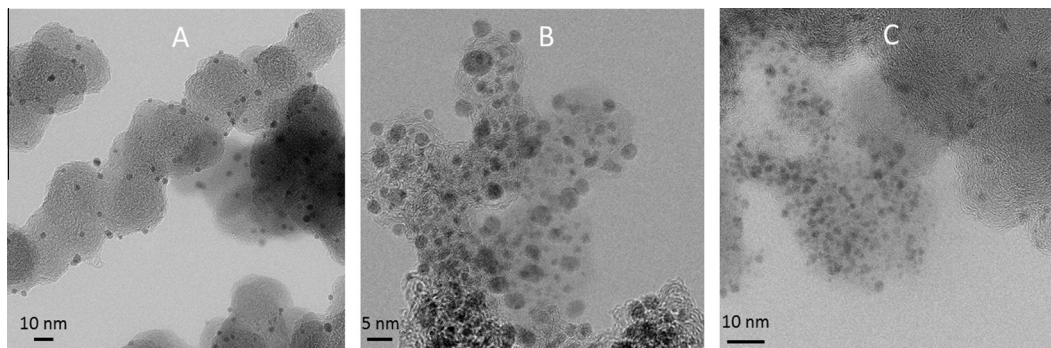


Fig. 2. HRTEM images of the ALD-prepared Pt (A), PtCo (B), and PtCoPt (C) catalysts.

and therefore Pt loading of this catalyst is slightly lower. Nevertheless, it has been ensured that the Co/Pt ratio in this catalyst remains the same as in the firstly made PtCo (ALD) catalyst (Table 1).

All of the particles are relatively small and in the same size range (Table 1) confirming that the change in activity does not result only from difference in the particle size. In addition, Fig. 2 shows that the particles are well dispersed throughout the whole carbon support. For bimetallic catalysts, EDX analysis on various locations was also performed to verify that both metals are distributed evenly on the support material. The analysis confirmed that the Co/Pt ratio was consistent with the AES results reported in Table 1. For the ALD catalysts, more detailed physical characterization is presented elsewhere [40].

3.2. Electrochemical characterization

The cyclic voltammograms of the cleaned catalyst surfaces in alkaline media are presented in Fig. 3, and it can be seen that both monometallic Pt catalysts have similar behavior: with the positive-going scan, there is one clear peak around 0.27 V potential as well as a shoulder around 0.36 V potential. They correspond to hydrogen desorption on Pt(110) and Pt(100), respectively, observed more clearly on Pt nanoparticles without carbon support or ionomer [41]. Above 0.45 V, the OH^- adsorption on Pt surface initiates followed by the formation of irreversible PtO_x layer on both catalyst [42]. Nevertheless, with the Pt (ALD) catalyst, both hydrogen adsorption/desorption peaks and double layer current are higher in comparison with the commercial catalyst due to the lower metal loading [43]. It should be noted that the profiles are coincident if the current values at the double layer region at potential of 0.5 V

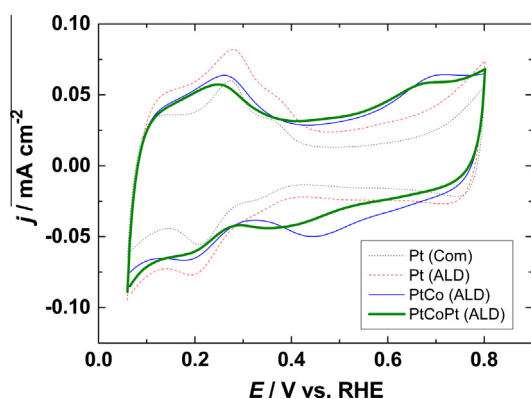


Fig. 3. Cyclic voltammograms of the cleaned catalyst surfaces in 0.1 mol dm^{-3} NaOH electrolyte with 50 mV s^{-1} scan rate.

are considered as baselines for Pt (Com) and Pt (ALD).

With bimetallic catalyst, the hydrogen adsorption/desorption is less defined and therefore only one clear hydrogen desorption peak is observed in Fig. 3 with the positive-going scan around potential of 0.25 V. In addition, the current for the double layer region increased and a peak above 0.65 V appears, and these both phenomena are associated with OH^- adsorption on Co or to CoO_x formation, whereas the corresponding CoO_x reduction is observed in the negative-going scan. Similar features have been reported for PtCo/C catalyst in KOH electrolyte [20,23,44,45]. When an additional layer of Pt is added the peak at high potential and the CoO_x reduction peak are shifted to less positive potentials implying that oxygenated species adsorb in a different way on this catalyst. The electrochemical durability of various ALD catalysts including Pt and Co was studied in acidic media elsewhere [40], and the results showed no indication that the Co would have been lost from the catalyst when the catalyst was cycled to 0.8 V. In alkaline media, bimetallic catalysts are often more stable confirming that these catalyst could be used also in DEFC anode conditions.

3.3. Ethanol oxidation

The activity of the ALD-prepared catalysts was studied for ethanol oxidation in alkaline media first with cyclic voltammetry, and the results obtained at 20°C are presented in Fig. 4, for clarity only the positive-going scans are shown. Fig. 4A and B presents the scans for still and rotating (1800 rpm) working electrodes, respectively, to facilitate the analysis of diffusion effects. The onset potential of ethanol oxidation was determined in both cases (with 0 and 1800 rpm rotation) by detecting the potential where the current was higher than the current caused by the hydrogen desorption in Fig. 3 (0.08 mA cm^{-2}), and the obtained values are presented in Table 2. In addition, currents for ethanol oxidation at the potentials of 0.5 and 0.8 V in Fig. 4 are also summarized in Table 2.

It can be seen from the Fig. 4A that Pt (Com) catalyst has the highest onset potential (0.56 V) similar to reported for Pt disk and Pt nanoparticle catalyst in alkaline media [23,46,47]. The reaction onset is reduced by 40 mV with the ALD-prepared Pt (Table 2), indicating that the higher order of the catalyst surface [40] increases the catalyst activity. In addition, the current produced in the whole potential range is higher with the Pt (ALD) catalyst than with Pt (Com). Nevertheless, the differences diminish when the working electrode is rotated (Fig. 4B), suggesting that the reactant diffusion to the stationary Pt (ALD) particles is more facile in comparison with the Pt (Com) particles. Similar observation has been made earlier with the ALD-prepared Pd catalyst [30].

It is evident on the basis of Table 2 and Fig. 4 that the onset potential of ethanol oxidation is clearly shifted to less-positive potentials by introduction of Co into the catalyst as also reported

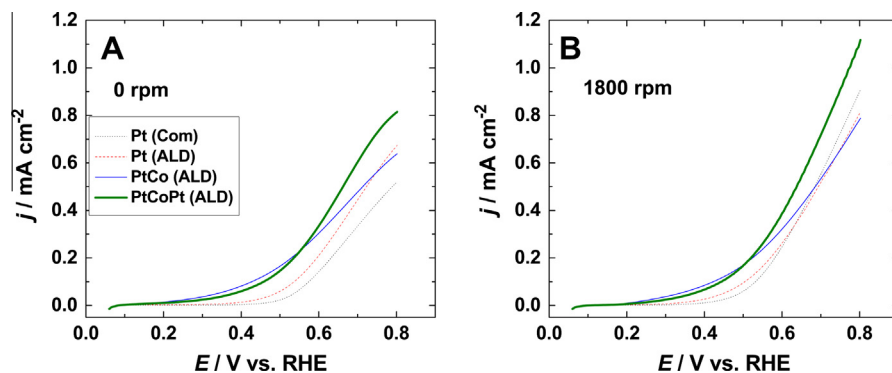


Fig. 4. Positive-going scans of the cyclic voltammetry for ethanol oxidation in solution of 1 mol dm^{-3} ethanol and 0.1 mol dm^{-3} NaOH (A) without rotation of the working electrode and (B) with 1800 rpm rotating, 10 mV s^{-1} scan rate at 20°C .

Table 2

The onset potential of ethanol oxidation and current values at 0.5 V potential, 20°C .

	E_{Onset} 0 rpm (V)	E_{Onset} 1800 rpm (V)	j at 0.5 V 1800 rpm (mA cm^{-2})	j at 0.8 V 1800 rpm (mA cm^{-2})
Pt (Com)	0.56	0.52	0.06	0.91
Pt (ALD)	0.52	0.49	0.10	0.81
PtCo (ALD)	0.40	0.39	0.17	0.79
PtCoPt (ALD)	0.43	0.42	0.17	1.11

previously [23], and this shift is independent of the diffusion because it can be observed both with and without rotation. When another Pt deposition cycle was performed on the PtCo catalyst, the onset shifted toward more positive potentials; thus, it is still clearly lower in comparison with pure Pt catalysts. As highlighted in Table 2, the current density obtained on the bimetallic catalysts at fuel cell relevant potential (0.5 V) is almost 3 times higher in comparison with Pt (Com). This increase in activity with bimetallic catalyst is in the same range as reported for this reaction on other bimetallic catalyst at this potential (2–5 times increase) [23,37,48,49]. At higher potentials, the PtCo (ALD) catalyst has lower performance than the monometallic Pt catalysts. Nevertheless, when additional Pt layer was placed on the top of the PtCo (ALD) catalyst, the performance remained superior in comparison with both Pt catalysts. This implies that the last layer of Pt atoms on the PtCoPt (ALD) catalyst is less prone to poisoning and simultaneously protecting the Co atoms still contributing with bi-functional mechanism. With both PtCo catalysts, an oxidation peak curve is visible below 0.8 V without rotation (Fig. 4A) indicating that the diffusion of reactants or reaction products starts to control at these potentials, though this is avoided with the rotation of the working electrode (Fig. 4B) or with a constant reactant flow at the DEFC anode.

Avoiding poisoning is essential for a catalytic material to be used in fuel cell applications. Ethanol oxidation occurs on the anode of a DEFC, and therefore, the potential of this electrode should be as low as possible to increase the total cell voltage. At a high voltage, the power obtained from the cell is not optimal and therefore a catalyst material that would oxidize efficiently ethanol at low potentials is of interest. To study the suitability of these catalysts for ethanol oxidation, potential step experiments of 30 min were performed at a potential of 0.5 V, relevant to a DEFC anode. The results obtained at 20°C are presented in Fig. 5.

As can be seen in Fig. 5, the current behavior and current degradation of both Pt catalysts is similar, suggesting that the reaction

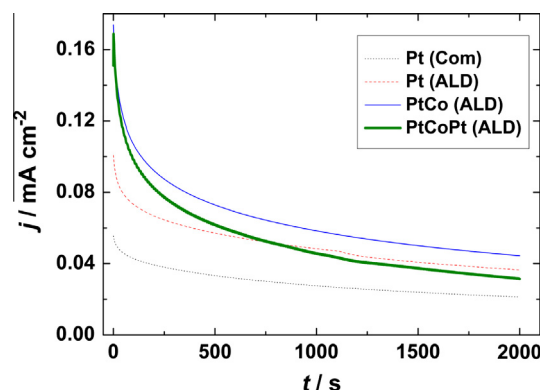


Fig. 5. Chronoamperometric curves for ethanol oxidation at 0.5 V potential in solution of 1 mol dm^{-3} ethanol and 0.1 M NaOH, with rotating working electrode (1800 rpm) at 20°C .

mechanism at 0.5 V potential is same; however, the current on Pt (ALD) was clearly higher throughout the experiment due to the more crystalline structure obtained by the ALD method [40]. With the bimetallic catalysts, the initial current was significantly higher, though the catalyst poisoning was more rapid than with the monometallic catalysts which may indicate that the reaction yielding poisoning species is enhanced. On PtCo (ALD), surface poisoning is less severe probably due to higher amount of Co atoms on the catalyst surface providing an oxygen source for the reaction intermediates inhibiting catalyst surface poisoning. The values for current densities obtained on PtCo (ALD) after 30 min of constant potential are over twice higher than on Pt (Com) that is one of the highest difference reported on bi- or trimetallic catalysts for this reaction [23,37,46,48]. Overall, the behavior of both bimetallic catalysts at this time scale differ in comparison with the pure Pt catalysts, and therefore, more detailed analysis of the reaction mechanism was performed with FTIR spectroscopy.

3.4. Reaction product analysis

In order to identify the species involved in the catalytic oxidation of ethanol on the ALD catalysts, IR experiments were performed. In the following spectra, the positive bands correspond to the products formed during ethanol oxidation, while negative bands arise due to the consumption of species present at the reference potential. The contact of the electrodes with the ethanol solution was performed at controlled potential (0.1 V) where, apparently, no adsorption or reaction process occurs [50]. This po-

tential was maintained until the electrode was pressed against the CaF₂ window. After collecting the reference spectrum, the potential was stepped progressively to higher potentials up to 0.8 V and then decreased stepwise again back to 0.1 V.

It is known that some of the possible products of ethanol oxidation can have vibrational band in a close range of wavenumbers. Therefore, the spectra obtained with an ATR configuration for acetate and acetaldehyde in a NaOH solution are presented in Fig. 6. This IR analysis was performed to determine the vibration frequencies of these species in alkaline solution. The NaOH solution was used as background meaning that the remaining bands will result from acetaldehyde or acetic acid in this media. From Fig. 6, it can be clearly observed that in contrast to acidic media [16], in alkaline media, both species have different vibrational bands. Acetate presents two major bands at 1553 and 1413 cm⁻¹ and a smaller one at 1357 cm⁻¹. For acetaldehyde, only one band at 1715 cm⁻¹ is observed. These results allow a clear distinction between the two products in the spectra obtained from potential controlled experiments.

The results obtained under controlled potential conditions for the ALD-prepared Pt and PtCo catalysts are presented in Fig. 7 where the sample potential of each spectrum is labeled, respectively. Several bands can be observed in the spectra represented in Fig. 7: a broad band between 2500 and 3000 cm⁻¹ was observed with all the studied surfaces. This band corresponds to the C–H region (2700–3000 cm⁻¹) and overlaps with other wide band denoting OH from carboxyl group between 2500 and 3000 cm⁻¹. This group is expected to exist in ethanol as well as in some of the most probable final products from its oxidation, like acetic acid [51]. These bands become more intense with the increase in the potential due to the higher oxidation rate. Other observed bands are the following: at 2341 cm⁻¹ the C–O asymmetric stretching from CO₂ [51,52]; at 1715 cm⁻¹ the C=O stretching of carbonyl groups from acetaldehyde (Fig. 7); the bands at 1553 and 1413 cm⁻¹ from O–C–O symmetric and asymmetry stretching (respectively) from acetate (Fig. 7) and at 1357 cm⁻¹ the CH₃ bending from acetate.

The observation of a band corresponding to CO₂ in alkaline media is unexpected because in this media the produced CO₂ would hydrolyze forming carbonate. However, during the ethanol oxidation, H⁺ is produced neutralizing the NaOH species given rise to changes in the local pH. In the particular case of thin layer con-

figurations (used in FTIR), the occurrence of local pH change is not surprising and would lead to the presence of CO₂ near the electrode surface. This fact was also described for ethanol oxidation in alkaline media on Pd surfaces [53].

All the surfaces have common bands at 1715 cm⁻¹ from acetaldehyde and between 1560 and 1350 cm⁻¹ due to acetate suggesting that both are reaction products in the studied catalysts independently of the presence of Co on the surface. However, a main difference can be observed between Pt and the two catalysts containing Co in the region correspondent to CO₂ production. It is important to notice that CO is not observed on any of the surfaces in the potential range studied. This fact does not mean that CO is absent under these conditions but more likely that the CO oxidation at these potentials is faster than its production and the corresponding IR bands stay below the detection limit. Moreover, it is well known that surface steps/defects enhance the rate of the CO oxidation on platinum surfaces [54,15,55]. On Pt nanoparticles, the CO oxidation to CO₂ is expected to be fast due to the small size of the crystalline sites and because the catalyst surface is formed in majority by defects and steps [54]. The absence of CO in the spectra obtained for ethanol oxidation on Pt-supported nanoparticles was also reported previously by our group for other catalysts [40].

The CO₂ band was only observed for the catalysts containing Co suggesting that this metal plays a key role in the splitting of the C–C bond that would lead to a more efficient total oxidation of ethanol. In addition, it is important to remark that with PtCo (ALD) (when Co is present), ethanol oxidation reaction starts earlier as it was observed in the cyclic voltammetry (Fig. 4) by the shift of the onset potential toward lower values and by the bands from acetate and acetaldehyde that appear at potentials as low as 0.4 V for this catalyst. These bands are also observed with the PtCoPt (ALD) catalyst, but they are less intense and are totally absent with the pure Pt catalyst. These results indicate that on pure Pt surface, the oxidation current observed is mainly contributed from the 4 e⁻ path, while in the case of PtCo catalysts also the 12 e⁻ path is involved. Nevertheless, even on pure Pt catalyst, the 12 e⁻ path should not be excluded because when small amount of CO₂ is produced it will be hydrolyzed to carbonate that cannot be distinguish by IR because overlapping of the carbonate (1390 cm⁻¹) and acetate bands. The FTIR results are summarized in Fig. 8 that plots the band area for CO₂ (2341 cm⁻¹), acetaldehyde (1715 cm⁻¹), and acetate (1553 cm⁻¹) against the applied potential for the three catalysts. The areas were obtained by fitting and deconvolution of the spectra shown in Fig. 7.

On the basis of Fig. 8, it is definitely concluded that with both the bimetallic PtCo catalysts, CO₂ is obtained as a final product from ethanol oxidation. The fact that the amount of CO₂ decreases with additional Pt cycle supports the theory that some of this Pt is deposited as a second layer on the pre-existent PtCo particles. This surface Pt could be poisoned, thus leading to a decrease in the catalyst activity. However, it should be remarked that this catalyst is still more active than pure Pt. The higher activity can also be observed by the higher integrated area for both acetaldehyde and acetate products at PtCoPt (ALD), and these results being in agreement with data from cyclic voltammetry (Fig. 4). At high potentials, the current on the PtCo (ALD) catalyst is lower than on catalyst with additional Pt cycle on the surface. It is also important to mention that acetaldehyde production is higher for PtCo (ALD) in the positive-going scan and it decreases very fast in the negative-going scan although the currents in the CV are still high. This decrease can be tentatively explained by the high CO₂ amount for this catalyst, meaning that probably acetaldehyde is being further oxidized to CO₂ at the negative-going scan.

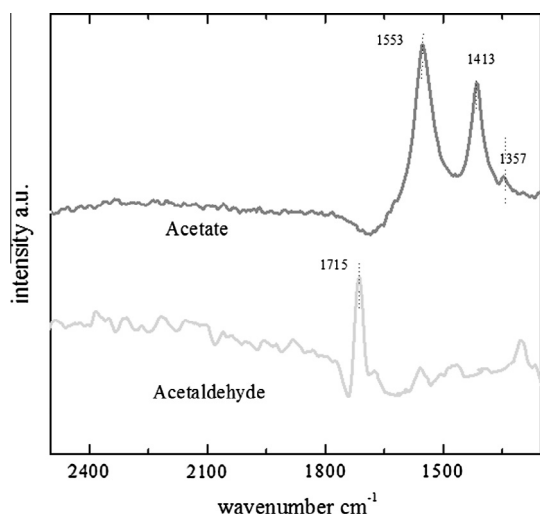


Fig. 6. ATR spectra of 0.1 mol dm⁻³ acetate and 0.1 mol dm⁻³ acetaldehyde in 0.1 mol dm⁻³ NaOH, 100 scans and 8 cm⁻¹, p-polarized light. Reference spectra: 0.1 mol dm⁻³ NaOH.

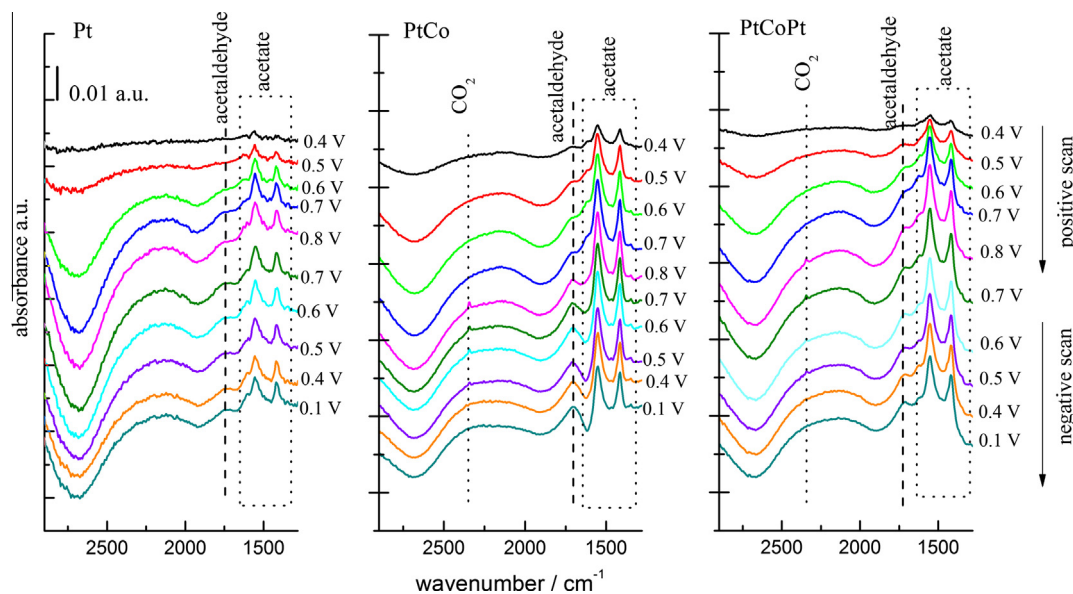


Fig. 7. Spectra obtained for ethanol oxidation on Pt (ALD), PtCo (ALD), and PtCoPt (ALD) catalysts in solution of 1 mol dm⁻³ ethanol and 0.1 mol dm⁻³ NaOH with 100 scans and 8 cm⁻¹ of resolution. Potential of each spectrum is indicated in the Figure. Reference spectra were obtained at 0.1 V.

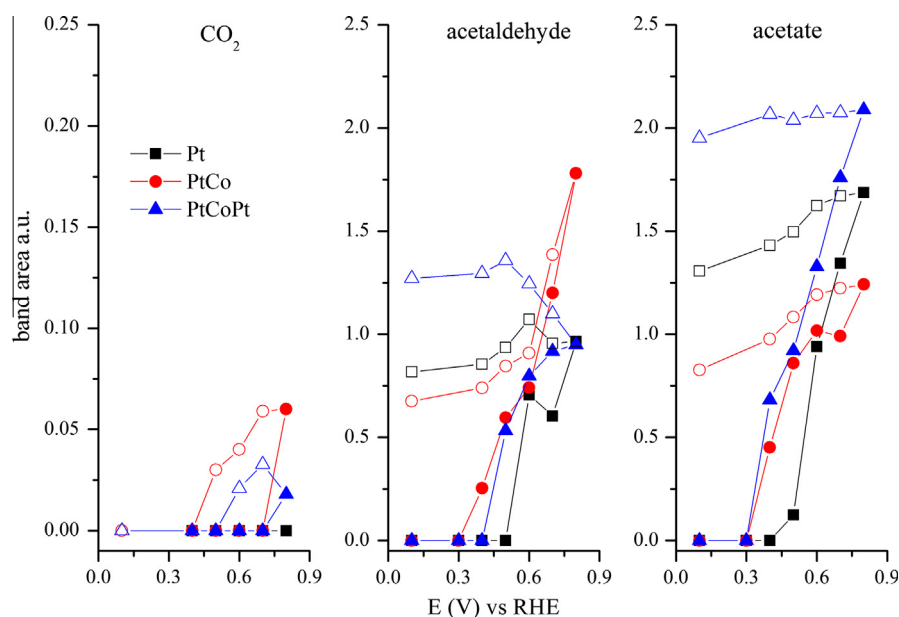


Fig. 8. Area of the bands for CO₂ (2341 cm⁻¹), acetaldehyde (1715 cm⁻¹), and acetate (1553 cm⁻¹) for Pt (ALD), PtCo (ALD), and PtCoPt (ALD). Colored and open symbols refer to values obtained with positive- and negative-going scans, respectively.

3.5. Temperature dependency

For portable DEFC applications, the operation temperature could vary from 0 to 60 °C and the activity for ethanol oxidation on the catalysts is presented at this temperature range in Fig. 9. The Fig. 9 shows that the ethanol oxidation is enhanced with increasing temperature as expected. However, the shape of the voltammogram at this potential region is not changed by temperature. The most important observation from Fig. 9 is that the Pt (Com) catalyst has the lowest variation with the temperature but with the ALD-prepared catalysts, the current increase with the temperature seems to be more significant.

For ethanol oxidation, the currents obtained at the negative-going scans are often higher than the ones obtained with the posi-

tive-going scans. This hysteresis mainly occurs when the catalyst surface is blocked by poisoning reaction intermediates that are only oxidized further at the highest potential of the cyclic voltammetry enabling the adsorption and oxidation of new reactants. In the temperature-dependent experiments, this is especially observed on all the catalyst with cycles performed at 0 °C (Fig. 9) due to the slow reaction kinetics. However, at this temperature, the hysteresis is lower with the bimetallic catalyst, implying that Co provides the opportunity for the intermediates to be oxidized further at lower potential and thus decreasing the poisoning. Nevertheless, with the bimetallic catalysts, the hysteresis is observed at elevated temperatures where very high current densities are observed. As it was seen in the chronoamperometric experiments (Fig. 5), the bimetallic surfaces suffer more from severe poisoning

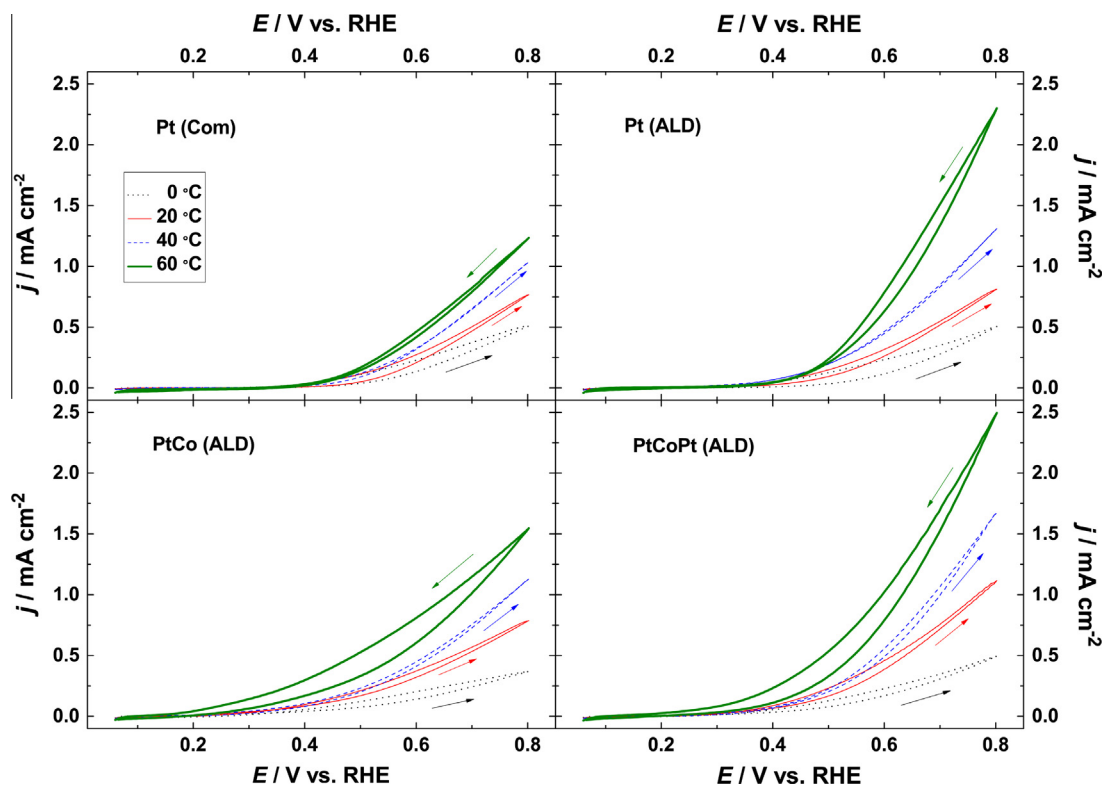


Fig. 9. Cyclic voltammograms of ethanol oxidation at various temperatures in solution of 1 mol dm^{-3} ethanol and 0.1 mol dm^{-3} NaOH. 10 mV s^{-1} scan rate with rotating working electrode (1800 rpm).

and the increase in the reaction rate with the temperature leads to increased poisoning of the surface sites further increasing hysteresis. To compare the changes in the onset potentials with the temperature, the potential values at the current of 0.08 mA cm^{-2} (from Fig. 9) are summarized in Table 3.

The trends of the onset potentials as a function of temperature in Table 3 are clear: firstly, the onset potential of all the catalysts decrease with the increase in temperature due to the enhancement of the reaction rate. Secondly, although the onset potential for ethanol oxidation reaction over the pure Pt surfaces occurs at 0.56 V at 0 °C , the potential decrease as a function of temperature is sharper with the Pt (ALD) catalyst, implying that at higher temperatures, this reaction is enhanced, as expected. Moreover, the onset potential of ethanol oxidation is shifted to less positive values at all the temperatures with the bimetallic catalysts reflecting that the addition of Co provides OH groups on the catalyst surface enabling total oxidation of ethanol at lower potential. The shift in the onset potential due to the Co addition with ALD process is $70\text{--}130 \text{ mV}$, depending on the temperature, whereas for the traditionally prepared Pt and PtCo catalysts, a shift of $20\text{--}70 \text{ mV}$ has been reported [23]. With additional Pt cycles on the bimetallic catalyst, the onset potential shifts closer to values of pure Pt surfaces

Table 3
The onset potential of ethanol oxidation at various temperatures.

	E_{Onset} at 0 °C 1800 rpm (V)	E_{Onset} at 20 °C 1800 rpm (V)	E_{Onset} at 40 °C 1800 rpm (V)	E_{Onset} at 60 °C 1800 rpm (V)
Pt (Com)	0.56	0.52	0.49	0.46
Pt (ALD)	0.56	0.49	0.44	0.41
PtCo (ALD)	0.43	0.39	0.37	0.32
PtCoPt (ALD)	0.44	0.42	0.41	0.37

at all the temperatures supporting the previous assumption that there are some Pt atoms covering the active surface sites in the PtCoPt (ALD) catalyst. These results strongly support the claim that with the ALD method, a preparation of structured bimetallic catalysts having Pt on top of some Co sites can be obtained and that these catalysts have superior performance compared to the traditionally prepared bimetallic catalysts. The poisoning behavior of these catalysts has been further studied with short potentials step experiments at various potentials because these experiments have shown to have better correspondence with the results from direct alcohol fuel cells [37]. The results are presented in Fig. 10 as a current density values obtained after applying a constant potential for 300 s as a function of the applied potential.

It should be noticed that in Fig. 10, scales for all the temperatures are the same, and therefore, at the lower temperatures, the changes between catalysts seem less dramatic; nevertheless, they are significant. At very low temperature (0 °C), there was hardly any current produced below 0.5 V . However, at higher potentials, the differences between the catalyst materials are remarkable: the current density produced with the Pt (Com) catalyst at the highest potential (0.8 V) is 1.5 times higher than that produced by the Pt (ALD) or PtCoPt (ALD) catalyst and more than 3 times higher produced by the PtCo (ALD) catalyst. This could indicate that the annealing of the catalyst would improve its properties at the lower temperatures.

Around the room temperature, current was produced with the bimetallic catalyst already at low potential region ($<0.6 \text{ V}$) as also observed earlier in Fig. 4. At this region, the Pt (ALD) catalyst produced notable current when on Pt (Com) only minor currents are observed below 0.6 V . Nevertheless, at higher potentials, more poisoning reaction products were formed on bimetallic catalyst surfaces and the current obtained after 300 s was lower than in the case of the pure Pt catalysts (Fig. 10). The most likely poisons

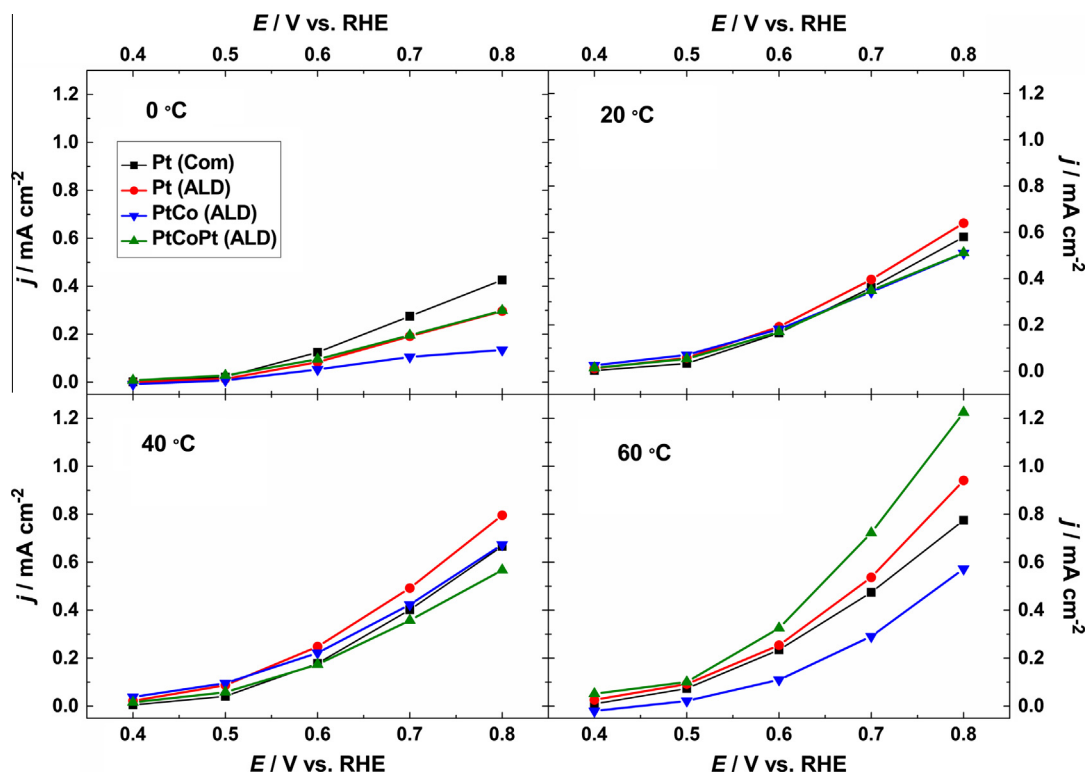


Fig. 10. Currents obtained after 300 s of potential step at selected potentials for ethanol oxidation in solution of 1 mol dm^{-3} ethanol and 0.1 mol dm^{-3} NaOH. The lines are added as a guide for the eye.

on a Pt-based catalyst at this potential region are acetaldehyde, acetone, and CO of which two first were observed on all the studied catalyst surfaces with the FTIR analysis (Fig. 7). The bimetallic surfaces seem to be poisoned faster than the pure Pt ones indicating that they promote more the formation of poisoning species. Observing CO_2 only at the potential of 0.8 V on the bimetallic surfaces suggests that there is also some formation of CO at these lower potentials although it was not observed in the FTIR experiments in Fig. 7 (likely because the amounts were under the detection limit).

When temperatures are further increased to 40 °C (Fig. 10), only a slight increase in the performance on all the catalyst is observed and this effect is most visible at the low potential region (below 0.6 V). The largest differences between the catalysts are observed at the high temperature (60 °C): both monometallic Pt catalysts perform similarly at lower potentials, however, at potentials higher than 0.6 V the Pt (ALD) catalyst exhibits increased performance. At 60 °C, PtCoPt (ALD) shows superior performance throughout the whole potential region confirming that this catalyst is not only stable but also active for ethanol oxidation at higher temperatures. In contrast, the PtCo (ALD) catalyst shows lower activity for ethanol oxidation at 60 °C than at 40 °C, and therefore, it cannot be totally ruled out that at 60 °C, some dissolution of Co from the surface of the PtCo (ALD) catalyst could occur. This fact underlines the importance of the protection of the bimetallic catalysts with additional Pt cycles.

3.6. Activation energies

To obtain more information of the temperature effects, Arrhenius analysis of the electrochemical data from Fig. 3 was performed (Supporting information, Figs. S1–S3) and the activation energies (E_a) as a function of the applied potential are shown in Fig. 11. In order to identify the limiting factors of ethanol oxidation, this anal-

ysis was performed by using the cyclic voltammetry data instead of potential step experiments, in which strong catalyst poisoning would affect the results. The currents were collected from the third scan of the cyclic voltammetry curves at slow scan rate (10 mV s^{-1}) and from the negative-going scan, in order to minimize the effect of anion and water adsorption as well as catalyst poisoning [56]. In addition, the values were taken from experiments where the working electrode was rotated to ensure that there are no bubbles covering the surface especially at the elevated temperatures and to minimize the diffusion limitations. It was demonstrated earlier that the activation energies do not depend on the WE rotation rate [56]. For the analysis of the PtCo (ALD) catalyst, the values at 60 °C

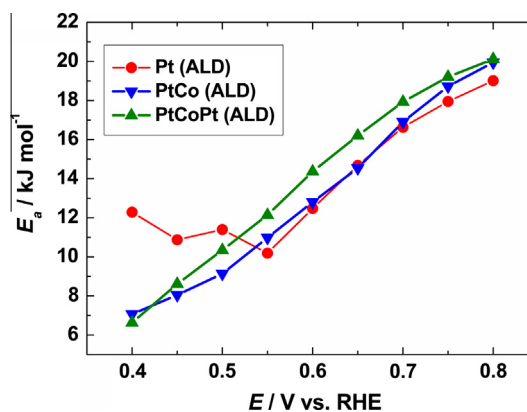


Fig. 11. The activation energies for ethanol oxidation at various potentials obtained from the Arrhenius plots (Figs. S1–S3). The values base on the negative-going scans of the cyclic voltammetry presented in Fig. 9 and the lines are added as a guide for the eye.

were discarded to ensure that the values are describing ethanol oxidation and not Co dissolution.

Overall, Fig. 11 shows that the activation energies for ethanol oxidation on the ALD-prepared catalysts are low (7–20 kJ mol⁻¹) and in agreement with those reported for ethanol oxidation over Pt nanoparticle catalysts in a NaOH solution [46,57,58]. However, the previously reported values were less potential dependent that might be due to the fact that the curves were analyzed by using currents recorded at the positive-going scan of ethanol oxidation. As pointed out by Cohen et al. [56] especially in alkaline media, the difference between values obtained with positive- and negative-going scans is significant, making the comparison of the values demanding.

For the Pt (ALD) catalyst, the activation energies decrease with the decrease in potential as expected for the negative-going scan until 0.55 V is reached. At the lower potentials, the activation energy continues to increase, indicating that a reaction barrier is faced that is most likely related to the availability of the OH-groups on the catalyst surface. With the bimetallic catalysts, almost linear activation energy dependency throughout the potential range is shown. This result suggests that at this potential range, the reaction mechanism remains the same as suggested the reaction product distribution in Fig. 8. Even though the FTIR analysis showed (Fig. 8) that less CO₂ was produced over the PtCoPt (ALD) catalyst, the *E_a* values obtained for PtCoPt (ALD) resemble more those of PtCo (ALD) than Pt (ALD), suggesting that the reaction mechanism is similar to the bimetallic PtCo (ALD) catalyst. This would support the conclusion that the structural PtCoPt (ALD) catalyst produces similar activity as bimetallic catalyst but has superior stability at the high temperatures.

As discussed in Section 3.4, CO₂ produced in an alkaline electrolyte will react to carbonate; however, the IR bands of carbonate overlap with the acetate and therefore cannot be distinguish. On the bimetallic catalyst, also traces of CO₂ are observed associated with a high production rate in the thin layer configuration where all CO₂ is not instantly carbonated. This implies that FTIR cannot exclude CO₂ production from ethanol oxidation in an alkaline media, and therefore, CO₂ production also on the Pt catalyst cannot be ruled out. The activation energies for ethanol oxidation on all of the ALD-prepared catalysts (Fig. 11) seem to be similar above 0.55 V that might suggests that ethanol is totally oxidized also on Pt (ALD) even though the CO₂ amounts produced are not high enough to be detected with FTIR in an alkaline electrolyte.

4. Conclusion

In this paper, Pt, PtCo, and PtCoPt catalysts were prepared by ALD and their activities for ethanol oxidation at a wide range of temperatures are evaluated. At the room temperature, the Pt (ALD) catalyst showed increased activity per Pt surface area in comparison with commercial Pt (Com) catalyst and this can be associated with a more carefully controlled synthesis resulting in more crystalline structure. Introduction of Co ALD cycles to form bimetallic catalyst enhanced ethanol oxidation, which could be demonstrated by a decrease in the onset potential and the increase in oxidation current at low overpotentials; however, the poisoning of the catalyst surfaces was accelerated. When an additional cycle of Pt was introduced on the bimetallic catalyst, the onset potential shifted toward values more Pt like; thus, the current densities on PtCoPt (ALD) were further increased.

The FTIR reaction product analysis confirmed that with both bimetallic PtCo catalysts, CO₂ is detected as an additional final product; however, it was not observed with the pure Pt catalyst. This suggests that the addition of Co enhances the mechanism toward to 12 e⁻ path, while on a pure Pt surface, the current is

mainly produced by the 4 e⁻ path. The activation energies obtained for the ALD catalyst showed that the PtCoPt (ALD) catalyst possess more bimetallic-like properties than Pt-like properties, confirming that the Co under the surface can still contribute via bi-functional mechanism. Especially at the elevated temperatures, the stability of the bimetallic catalyst remains as an issue even in an alkaline media and therefore the protection of the bimetallic catalyst is important. PtCoPt catalyst prepared by the ALD method showed significant increase in stability at the high temperatures. The results clearly demonstrate that the bimetallic catalyst having three deposition cycles alternating with Pt and Co show both increased activity and durability in comparison with traditional bimetallic catalysts.

Acknowledgements

The authors acknowledge Aalto University and Academy of Finland for funding. Matti Aarnio is acknowledged for providing the images of the cell configuration.

Appendix A. Supplementary material

Supplementary data associated with this article can be found, in the online version, at <http://dx.doi.org/10.1016/j.jcat.2013.08.027>.

References

- [1] C. Lamy, E.M. Belgsir, J.-M. Leger, *J. Appl. Electrochem.* 31 (2001) 799.
- [2] A. Santasalo, T. Kallio, K. Kontturi, *Platinum Metals Rev.* 53 (2009) 58.
- [3] J.R. Varcoe, R.C.T. Slade, E.L.H. Yee, S.D. Poynton, D.J. Driscoll, *J. Power Sources* 173 (2007) 194.
- [4] C. Lamy, J.-M. Leger, S. Srinivasan, in: J.O'M. Bockris, B.E. Conway, R.E. White (Eds.), *Modern Aspects of Electrochemistry*, vol. 32, Kluwer Academic/Plenum Publishers, New York, 2001, p. 65.
- [5] S.C.S. Lai, M.T.M. Koper, *Phys. Chem. Chem. Phys.* 11 (2009) 10446.
- [6] J.S. Spendelov, A. Wieckowski, *Phys. Chem. Chem. Phys.* 9 (2007) 2654.
- [7] G. Cui, S. Song, P.K. Shen, A. Kowal, C. Bianchini, *J. Phys. Chem. C* 113 (2009) 15639.
- [8] A. Santasalo-Aarnio, S. Hietala, T. Rauhama, T. Kallio, *J. Power Sources* 196 (2011) 6153.
- [9] H. Bunazawa, Y. Yamazaki, *J. Power Sources* 190 (2009) 210.
- [10] J.R. Varcoe, R.C.T. Slade, *Fuel Cells* 5 (2005) 187.
- [11] N. Fujiwara, Z. Siroma, S. Yamazaki, T. Ioroi, H. Senoh, K. Yasuda, *J. Power Sources* 185 (2008) 621.
- [12] Y.S. Li, T.S. Zhao, Z.X. Liang, *J. Power Sources* 190 (2009) 223.
- [13] V. Bambagioni, C. Bianchini, A. Marchionni, J. Filippi, F. Vizza, J. Teddy, P. Serp, M. Zhiani, *J. Power Sources* 190 (2009) 241.
- [14] U. Schmiemann, U. Muller, H. Baltruschat, *Electrochim. Acta* 40 (1995) 99.
- [15] J. Shin, W.J. Tornquist, C. Korzeniewski, C.S. Hoaglund, *Surf. Sci.* 364 (1996) 122.
- [16] F. Colmati, G. Tremiliosi-Filho, E.R. Gonzalez, A. Berna, E. Herrero, J.M. Feliu, *Faraday Discuss.* 140 (2009) 379.
- [17] D. Bayer, S. Berenger, C. Cremers, J. Tubke, *ECS Trans.* 25 (2010) 95.
- [18] O.A. Petrii, B.I. Podlovchenko, A.N. Frumkin, H. Lal, *J. Electroanal. Chem.* 10 (1965) 253.
- [19] T. Frelink, W. Visscher, J.A.R. van Veen, *Surf. Sci.* 335 (1995) 353.
- [20] C. Wang, N.M. Markovic, V.R. Stamenkovic, *ACS Catal.* 2 (2012) 891.
- [21] S. Koh, C. Yu, P. Mani, R. Srivastava, P. Strasser, *J. Power Sources* 172 (2007) 50.
- [22] M. Oezaslan, F. Hasche, P. Strasser, *J. Electrochem. Soc.* 159 (2012) B394.
- [23] C. Xu, Y. Su, L. Tan, J. Zhang, S. Chen, S.P. Jiang, *Electrochim. Acta* 54 (2009) 6322.
- [24] H. Zhao, J. Dong, S. Xing, Y. Li, J. Shen, J. Xu, *Int. J. Hydrogen Energy* 36 (2011) 9551.
- [25] H. Huang, Y. Fan, X. Wang, *Electrochim. Acta* 80 (2012) 118.
- [26] P. Hernandez-Fernandez, M. Montiel, P. Ocon, J.L.G. Fierro, H. Wang, H.D. Abruña, S. Rojas, *J. Power Sources* 195 (2010) 7959.
- [27] X. Zhang, H. Wang, J. Key, V. Linkov, S. Ji, X. Wang, Z. Lei, R. Wang, *J. Electrochem. Soc.* 159 (2012) B270.
- [28] H. Qiu, F. Zou, *Appl. Mater. Interfaces* 4 (2012) 1404.
- [29] S. Haukka, T. Suntola, *Int. Sci.* 5 (1997) 119.
- [30] E. Rikkinen, A. Santasalo-Aarnio, S. Airaksinen, M. Borghei, V. Viitanen, J. Sainio, E.I. Kauppinen, T. Kallio, A.O.I. Krause, *J. Phys. Chem. C* 115 (2011) 23067.
- [31] T. Shu, S.-J. Liao, C.-T. Hsieh, A.K. Roy, Y.-Y. Liu, D.-Y. Tzou, W.-Y. Chen, *Electrochim. Acta* 75 (2012) 101.
- [32] J. Li, X. Liang, D.M. King, Y.-B. Jiang, A.W. Weimer, *Appl. Catal. B: Environ.* 97 (2010) 220.

- [33] Y.-C. Hsued, C.-C. Wang, C.-C. Kei, Y.-H. Lin, C. Liu, T.-P. Perng, *J. Catal.* 294 (2012) 63.
- [34] S.T. Christensen, H. Feng, J.L. Libera, N. Guo, J.T. Miller, P.C. Stair, J.W. Elam, *Nano Lett.* 10 (2010) 3047.
- [35] X. Jiang, T.M. Gur, F.B. Prinz, S.F. Bent, *Chem. Matter.* 22 (2010) 3024.
- [36] Y. Lei, B. Liu, R.J. Lobo-Lapidus, T. Wu, H. Feng, X. Xia, A.U. Mane, J.L. Libera, J.P. Greeley, J.T. Miller, J.W. Elam, *Chem. Mater.* 24 (2012) 3525.
- [37] A. Santasalo-Aarnio, S. Tuomi, K. Jalkainen, K. Kontturi, T. Kallio, *Electrochim. Acta* 87 (2013) 730.
- [38] M. Figueiredo, V. Climent, J.M. Feliu, *Electrocatalysis* 2 (2011) 255.
- [39] M. Figueiredo, A. Santasalo-Aarnio, F. Vidal-Iglesias, J. Solla-Gullón, J.M. Feliu, K. Kontturi, T. Kallio, *Appl. Catal. B: Environ.* 140–141 (2013) 378.
- [40] E. Sairanen, M. Figueiredo, R. Karinen, A. Santasalo-Aarnio, H. Jiang, J. Sainio, T. Kallio, J. Lehtonen, *Appl. Catal. B: Environ.* (2013) (submitted for publication).
- [41] F.J. Vidal-Iglesias, R.M. Arán-Ais, J. Solla-Gullón, E. Herrero, J.M. Feliu, *ACS Catal.* 2 (2012) 901.
- [42] A.V. Tripkovic, K.Dj. Popovic, J.D. Lovic, V.M. Jovanovic, A. Kowal, *J. Electroanal. Chem.* 572 (2004) 119.
- [43] S. Chumillas, C. Buso-Rogero, J. Solla-Gullón, F.J. Vidal-Iglesias, E. Herrero, J.M. Feliu, *Electrochem. Commun.* 13 (2011) 1194.
- [44] Q. He, S. Mukerjee, *Electrochim. Acta* 55 (2010) 1709.
- [45] H. Schulenburg, J. Durst, E. Muller, A. Wokaun, G.G. Scherer, *J. Electroanal. Chem.* 642 (2010) 52.
- [46] J. Datta, A. Dutta, S. Mukherjee, *J. Phys. Chem. C* 115 (2011) 15324.
- [47] D. Bayer, S. Berenger, M. Joos, C. Cremers, J. Tubke, *Int. J. Hydrogen Energy* 35 (2010) 12660.
- [48] P.-C. Su, H.-S. Chen, T.-Y. Chen, C.-W. Liu, C.-H. Lee, J.-F. Lee, T.-S. Chan, K.-W. Wang, *Int. J. Hydrogen Energy* 38 (2013) 4474.
- [49] S.Y. Shen, T.S. Zhao, J.B. Xu, *Int. J. Hydrogen Energy* 35 (2010) 12911.
- [50] S.C.S. Lai, M.T.M. Koper, *Faraday Discuss.* 140 (2009) 399.
- [51] X.H. Xia, H.-D. Liess, T. Iwasita, *J. Electroanal. Chem.* 437 (1997) 233.
- [52] T. Iwasita, B. Rasch, E. Cattaneo, W. Vielstich, *Electrochim. Acta* 34 (1989) 1073.
- [53] Z. Zhou, Q. Wang, J. Lin, N. Tian, S. Sun, *Electrochim. Acta* 55 (2010) 7995.
- [54] Q. Chen, J. Solla-Gullón, S. Sun, J.M. Feliu, *Electrochim. Acta* 55 (2010) 7982.
- [55] D. Tarnowski, C. Korzeniewski, *J. Phys. Chem. B* 101 (1997) 253.
- [56] J.L. Cohen, D.J. Volpe, H.D. Abruña, *Phys. Chem. Chem. Phys.* 9 (2007) 49.
- [57] S.S. Mahapatra, A. Dutta, J. Datta, *Electrochim. Acta* 55 (2010) 9097.
- [58] A.V. Tripkovic, S. Strbac, K.Dj. Popovic, *Electrochem. Commun.* 5 (2003) 484.